OBSTACLES RECONSTRUCTION FROM PARTIAL BOUNDARY MEASUREMENTS BASED ON THE TOPOLOGICAL DERIVATIVE CONCEPT

S. S. ROCHA AND A.A. NOVOTNY

Abstract. In this work a new method for obstacles reconstruction from partial boundary measurements is proposed. For a given boundary excitation, we want to determine the quantity, locations and sizes of a number of holes embedded within a geometrical domain, from partial boundary measurements related to such an excitation. The resulting inverse problem is written in the form of an ill-posed and over-determined boundary value problem. The idea therefore is to rewrite it as an optimization problem where a shape functional measuring the misfit between the boundary measurement and the solution to an auxiliary boundary value problem is minimized with respect to a set of ball-shaped holes. The topological derivative concept is used for solving the associated topology optimization problem, leading to a second-order reconstruction algorithm. The resulting algorithm is non-iterative – and thus very robust with respect to noisy data – and also free of initial guess. Finally, some numerical results are presented in order to demonstrate the effectiveness of the proposed reconstruction algorithm.

1. Introduction

Inverse problems associated with anomalies detection such as cracks, cavities or inclusions have been subject of intense research over the last decades. As a result of the continuous research efforts in this direction a wide body of literature is currently available on these topics, namely: crack identification (Alves and Ha-Duong, 1999; Andrieux et al., 1999; Kress, 1996; Nishimura and Kobayashi, 1994), inverse scattering (Colton et al., 2003; Colton and Kirsch, 1996; Kress, 1995; Feijóo et al., 2004; Guzina and Bonnet, 2004), obstacle reconstruction (Alvarez et al., 2005; Caubet and Dambrine, 2012; Litman, 2005), inverse potential problem (Isakov, 1990; Leitão and Baumeister, 2005; Prilepko, 1974), for instance.

Among the methods dealing with inverse reconstruction problems available in the literature we highlight the level-set method and the methods based on asymptotic expansions. The level-set method used for example by Burger (2001); Doel et al. (2010); Dorn and Lesselier (2006) can be seen as a first-order iterative method, whose solution is usually dependent on the initial guess associated with the level-set initialization. The asymptotic analysis is often used to describe asymptotic behavior of solutions to boundary value problems. Thus, an important class of methods are based on asymptotic expansions (Ammari and Kang, 2004; Capdeboscq and Vogelius, 2003a,b; Cedio-Fengya et al., 1998; Liepa et al., 1993). More recently, the topological derivative concept (Sokołowski and Żochowski, 1999) has been proved to be useful in the solution of a wide class of reconstruction inverse problems. See, for instance the papers by Amstutz and Dominguez (2008); Amstutz et al. (2005); Bonnet (2006); Carpio and Rapún (2008); Dominguez et al. (2005); Guzina and Bonnet (2006); Guzina and Chikichev (2007). The topological derivative also leads to first-order iterative methods, but in contrast to the level-set methods, they are free of initial guess. In addition, the notion of second order topological derivative (de Faria and Novotny, 2009) has been used to devise a class of second order non-iterative methods (Bonnet, 2009; Canelas et al., 2014, 2015; Hintermüller et al., 2012).

Following the original ideas presented by de Faria and Novotny (2009), in this paper a new method for solving an inverse obstacle reconstruction problem from partial boundary measurements is proposed. In particular, for a given boundary excitation, we want to determine the quantity, locations and sizes of a number of holes embedded within a geometrical domain, from partial boundary measurements related to such an excitation. The resulting inverse problem is written in the form of an ill-posed and over-determined boundary value problem. The idea therefore is to rewrite it as an optimization problem where a shape functional measuring the misfit between the boundary measurement and the solution to an auxiliary boundary value problem is minimized with respect to a set of ball-shaped holes. The second order topological derivative concept is used for solving the associated topology optimization problem, leading to a second-order reconstruction algorithm. In particular, we recover a term which is frequently disregarded in the literature and show that it is actually crucial for solving the inverse problem we are dealing with.

Key words and phrases. obstacles reconstruction, inverse problem, topological asymptotic analysis.

In contrast to existing approaches, the resulting algorithm is non-iterative - and thus very robust with respect to noisy data - and also free of initial guess. Finally, some numerical results are presented in order to demonstrate the effectiveness of the proposed reconstruction algorithm.

The paper is organized as follows. In Section 2 the inverse model problem we are dealing with is stated, which is rewritten in the form of a topology optimization problem. The associated topological asymptotic analysis is developed in all details in Section 3, were the resulting reconstruction algorithm is devised. In Section 4, some numerical experiments are presented in order to show the effectiveness and robustness of the reconstruction algorithm. Finally, the paper ends with some concluding remarks and new perspectives in Section 5.

2. Problem Formulation

Let $\mathcal{D} \subset \mathbb{R}^2$ be an open and bounded domain with smooth boundary Γ_m. We introduce a subset Ω of $\mathcal{D}$ such that $\Omega = \mathcal{D} \setminus \overline{\omega_0}$, with $\omega_0 \Subset \mathcal{D}$. The boundary of Ω is split into two disjoints boundaries Γ_m and Γ_0, where Γ_0 is used to denote the boundary of the hole ω_0. Let us consider the domain $\Omega^* = \Omega \setminus \overline{\omega^*}$, where $\omega^* \Subset \Omega$ represents a number $N^* \in \mathbb{N}$ of unknown holes (obstacles) within Ω^*. The boundary of Ω^* is split into three disjoints subsets Γ_m, Γ_0 and $\partial\omega^*$, where $\partial\omega^*$ is used to denote the boundaries of the N^* obstacles ω^*. See sketch in Fig. 1. The inverse problem we are dealing with consists in finding ω^* such that the following over-determined boundary value problem is satisfied:

$$\left\{\begin{array}{rcll} \Delta u &=& 0 & \text{in } \Omega^*, \\ u &=& 0 & \text{on } \Gamma_0, \\ u &=& 0 & \text{on } \partial\omega^*, \\ u &=& U & \\ -\partial_n u &=& Q & \text{on } \Gamma_m, \end{array}\right. \tag{2.1}$$

where U and Q are the Cauchy data on Γ_m. We assume that the flux Q is imposed while the potential U is written.

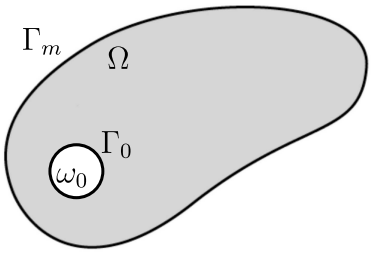

(a) domain without obstacles

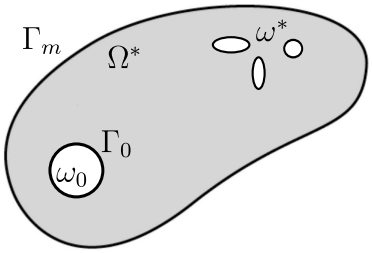

(b) domain with obstacles

Figure 1. Domains Ω e Ω^*.

Since the inverse problem (2.1) is written in the form of an ill-posed and over-determined boundary value problem, the idea is to rewrite it as a topology optimization problem, namely

$$\underset{\Omega \subset \mathcal{D}}{\text{Minimize}} \quad \psi(\Omega) = \sum_{k=1}^{M} \int_{\Gamma_m} (u_0^k - U^k)^2, \tag{2.2}$$

where M is the number of partial boundary measurements. Some terms in the above minimization problem require explanation. The shape functional $\psi(\Omega)$ measures the misfit between each boundary measurement U^k and the trace on Γ_m of the solution to the following auxiliary boundary value problem depending on the boundary data Q^k

$$\left\{\begin{array}{rcll} \Delta u_0^k &=& 0 & \text{in } \Omega, \\ u_0^k &=& 0 & \text{on } \Gamma_0, \\ -\partial_n u_0^k &=& Q^k & \text{on } \Gamma_m, \end{array}\right. \tag{2.3}$$

where $u_0^k = u_0^k(\Omega)$. Note that over the solution to the inverse problem (2.1), namely $\Omega = \Omega^*$, the shape functional $\psi(\Omega^*)$ is minimized according to the topology optimization problem (2.2). See, for instance, the paper by Kohn and Vogelius (1984).

3. Topological Asymptotic Analysis

The topological derivative concept is used to solve problem (2.2), which has been specifically designed to deal with such a topology optimization problem (Novotny and Sokołowski, 2013). The idea is to perform the topological asymptotic analysis of the shape functional $\psi(\Omega)$ with respect to the insertion of a number $N \geq N^*$ of infinitesimal holes in the domain Ω. Therefore, let us introduce the

topologically perturbed counterpart of Ω given by $\Omega_\varepsilon = \Omega \backslash \bigcup_{i=1}^{N} \overline{B_{\varepsilon_i}}$, with $B_{\varepsilon_i} \cap B_{\varepsilon_j} = \emptyset$ for $i \neq j$, where $B_{\varepsilon_i} = B(x_i, \varepsilon_i) \Subset \Omega$ is a ball of center at $x_i \in \Omega$ and radius ε_i. The shape functional associated with the topologically perturbed domain Ω_ε is written as

$$\psi(\Omega_\varepsilon) = \sum_{k=1}^{M} \int_{\Gamma_m} (u_\varepsilon^k - U^k)^2, \tag{3.1}$$

with $u_\varepsilon^k = u_\varepsilon^k(\Omega_\varepsilon)$ solution to the following perturbed boundary value problem

$$\left\{ \begin{array}{rcll} \Delta u_\varepsilon^k &=& 0 & \text{in } \Omega_\varepsilon, \\ u_\varepsilon^k &=& 0 & \text{on } \Gamma_0, \\ -\partial_n u_\varepsilon^k &=& Q^k & \text{on } \Gamma_m, \\ u_\varepsilon^k &=& 0 & \text{on } \bigcup_{i=1}^{N} \partial B_{\varepsilon_i}, \end{array} \right. \tag{3.2}$$

where $\varepsilon = \{\varepsilon_1, \varepsilon_2, \ldots, \varepsilon_N\} \in \mathbb{R}_+^N$.

3.1. **Asymptotic Analysis of the Solution.** The perturbed shape functional $\psi(\Omega_\varepsilon)$ given by (3.1) depends on the small parameter ε through the solution u_ε^k of (3.2). Therefore, following the original ideas developed in the book by Mazya et al. (2000), we start by considering the following ansätz for the expansion of u_ε^k with respect to ε (see also Kozlov et al. (1999)),

$$u_\varepsilon^k(x) = u_0^k(x) + \sum_{j=1}^{N} \varphi_{\varepsilon_j}^k(x) + \tilde{u}_\varepsilon^k(x), x \in \Omega_\varepsilon, \tag{3.3}$$

with $\varphi_{\varepsilon_j}^k(x) = \alpha_j^k(\varepsilon_j) G_j(x)$, where $G_j(x)$ is the associated Green's function, solution of the following boundary value problem

$$\left\{ \begin{array}{rcll} -\Delta G_j &=& \delta_j & \text{in } \Omega, \\ \partial_n G_j &=& 0 & \text{on } \Gamma_m, \\ G_j &=& 0 & \text{on } \Gamma_0, \end{array} \right. \tag{3.4}$$

where $\delta_j := \delta(x - x_j)$, with δ used to denote the Dirac delta distribution. In the neighborhood of $x_j \in \Omega$, function G_j admits the following representation

$$G_j(x) = \phi_j(x) - g_j(x), \tag{3.5}$$

where $\phi_j(x) = (2\pi)^{-1} \ln \|x - x_j\|$ is the fundamental solution for the Laplacian into two spacial dimensions and $g_j(x)$ is the regular part of the Green's function, solution of the following auxiliary boundary value problem

$$\left\{ \begin{array}{rcll} \Delta g_j &=& 0 & \text{in } \Omega, \\ \partial_n g_j &=& \partial_n \phi_j & \text{on } \Gamma_m, \\ g_j &=& \phi_j & \text{on } \Gamma_0. \end{array} \right. \tag{3.6}$$

Remark 1. *Note that $g_j(x) = g_j(x; x_j)$, because $\phi_j(x) = \phi_j(x; x_j)$ depends on the point x_j where the hole is nucleated. It means that function $g_j(x)$ depends on x_j, this implies that the complexity order associated with the computation of all g_j becomes very high. However, we will show through some numerical experiments that this term is crucial for solving the topology optimization problem* (2.2) *or equivalently the inverse problem* (2.1)*. Since the term $g_j(x)$ is frequently disregarded in the literature, then the study of its role in the reconstruction of the hidden obstacles ω^* from partial boundary measurement can be seen as the main theoretical contribution of this paper.*

Let us expand $u_0^k(x)$ and $g_j(x)$ in Taylor's series around the point x_i, which allows to rewrite (3.3) as follows

$$\begin{aligned} u_\varepsilon^k(x) &= u_0^k(x_i) + \nabla u_0^k(y_i) \cdot (x - x_i) \\ &+ \sum_{j=1}^{N} \alpha_j^k(\varepsilon_j) \left(\phi_j(x) - g_j(x_i) - \nabla g_j(z_i) \cdot (x - x_i) \right) \\ &+ \tilde{u}_\varepsilon^k(x), \end{aligned} \tag{3.7}$$

where y_i and z_i are intermediate points between x and x_i. On the boundary of the hole $\partial B_{\varepsilon_i}$ we have $u_\varepsilon^k = 0$ and $x = x_i - \varepsilon_i n_i$, where n_i is the unit normal vector pointing toward the center of the circular hole B_{ε_i}. Thus the expansion for u_ε^k, evaluated on $\partial B_{\varepsilon_i}$, leads to

$$\begin{aligned} u_\varepsilon^k(x)_{|_{\partial B_{\varepsilon_i}}} &= -\varepsilon_i \nabla u_0^k(y_i) \cdot n_i + \varepsilon_i \alpha_i^k(\varepsilon_i) \nabla g_i(z_i) \cdot n_i \\ &- \sum_{\substack{j=1 \\ j \neq i}}^{N} \alpha_j^k(\varepsilon_j) \left(\frac{1}{2\pi} \ln \|x_i - x_j\| + g_j(x_i) \right) + u_0^k(x_i) \\ &- \sum_{\substack{j=1 \\ j \neq i}}^{N} \alpha_j^k(\varepsilon_j) \left(\tilde{\varepsilon}_i \nabla \phi_j(x_i, x_j) + \varepsilon_i \nabla g_j(z_i) \right) \cdot n_i \\ &- \alpha_i^k(\varepsilon_i) \left(\frac{1}{2\pi} \ln \varepsilon_i + g_i(x_i) \right) + \tilde{u}_\varepsilon^k(x) = 0, \end{aligned} \tag{3.8}$$

with $0 < \tilde{\varepsilon}_i < \varepsilon_i$. We can choose $\widetilde{u}_\varepsilon^k$ on $\partial B_{\varepsilon_i}$, such that

$$\begin{aligned} \widetilde{u}_\varepsilon^k(x)_{|_{\partial B_{\varepsilon_i}}} &= \varepsilon_i \nabla u_0^k(y_i) \cdot n_i - \varepsilon_i \alpha_i^k(\varepsilon_i) \nabla g_i(z_i) \cdot n_i \\ &+ \sum_{\substack{j=1 \\ j \neq i}}^{N} \alpha_j^k(\varepsilon_j) \left(\tilde{\varepsilon}_i \nabla \phi_j(x_i, x_j) + \varepsilon_i \nabla g_j(z_i) \right) \cdot n_i. \end{aligned} \tag{3.9}$$

Consequently, $\alpha_i^k(\varepsilon_i)$ is solution to the following algebraic equation

$$\begin{aligned} u_0^k(x_i) - \alpha_i^k(\varepsilon_i) \left(\frac{1}{2\pi} \ln \varepsilon_i + g_i(x_i) \right) \\ - \sum_{\substack{j=1 \\ j \neq i}}^{N} \alpha_j^k(\varepsilon_j) \left(\frac{1}{2\pi} \ln \|x_i - x_j\| + g_j(x_i) \right) = 0. \end{aligned} \tag{3.10}$$

Finally, the remainder $\widetilde{u}_\varepsilon^k$ is constructed such that it compensates for the discrepancies introduced by

the Taylor's expansions of $u^k(x)$, $g_j(x)$ and $\phi_j(x)$. Therefore, $\widetilde{u}_\varepsilon^k$ must satisfy the following boundary value problem

$$\left\{\begin{array}{rcl} \Delta\widetilde{u}_\varepsilon^k &=& 0 \quad \text{in} \quad \Omega_\varepsilon, \\ \widetilde{u}_\varepsilon^k &=& 0 \quad \text{on} \quad \Gamma_0, \\ \partial_n\widetilde{u}_\varepsilon^k &=& 0 \quad \text{on} \quad \Gamma_m, \\ \widetilde{u}_\varepsilon^k &=& h_i \quad \text{on} \quad \bigcup_{i=1}^N \partial B_{\varepsilon_i}, \end{array}\right. \tag{3.11}$$

with function h_i defined as

$$\begin{aligned} h_i = \varepsilon_i(\nabla u_0^k(y_i) - \alpha_i^k(\varepsilon_i)\nabla g_i(z_i)) \cdot n_i \\ - \sum_{\substack{j=1 \\ j\neq i}}^N \alpha_j^k(\varepsilon_j)\left(\tilde{\varepsilon}_i \nabla\phi_j(x_i,x_j) + \varepsilon_i \nabla g_j(z_i)\right)\cdot n_i. \end{aligned} \tag{3.12}$$

3.2. **Asymptotic Analysis of the Shape Functional.** Now, we have all elements to evaluate the shape functional $\psi(\Omega_\varepsilon)$ explicitly. In fact, after introducing the ansätz (3.3) into (3.1), we have the following important result:

$$\begin{aligned} \psi(\Omega_\varepsilon) = \sum_{k=1}^M \int_{\Gamma_m} (u_0^k - U^k)^2 + \sum_{k=1}^M \mathcal{E}^k(\varepsilon) \\ + 2\sum_{k=1}^M \int_{\Gamma_m} (u_0^k - U^k) \sum_{j=1}^N \alpha_j^k(\varepsilon_j) G_j \\ + \sum_{k=1}^M \int_{\Gamma_m} \left(\sum_{j=1}^N \alpha_j^k(\varepsilon_j) G_j\right)^2 \end{aligned} \tag{3.13}$$

with the remainder

$$\begin{aligned} \mathcal{E}^k(\varepsilon) = 2\int_{\Gamma_m} (u_0^k - U^k)\widetilde{u}_\varepsilon^k \\ + 2\int_{\Gamma_m} \widetilde{u}_\varepsilon^k \sum_{j=1}^N \varphi_{\varepsilon_j}^k + \int_{\Gamma_m} (\widetilde{u}_\varepsilon^k)^2. \end{aligned} \tag{3.14}$$

Before proceeding, let us consider the particular case associated with just one hole and one boundary measurement. By setting $M = 1$ and $N = 1$ in (3.13), there is

$$\psi(\Omega_\varepsilon) = \psi(\Omega) + 2\alpha(\varepsilon)\int_{\Gamma_m} (u_0 - U)G + \mathcal{E}(\varepsilon), \tag{3.15}$$

with the remainder redefined as

$$\mathcal{E}(\varepsilon) = 2\int_{\Gamma_m} (u_0 - U)\widetilde{u}_\varepsilon + \int_{\Gamma_m} (\varphi_\varepsilon + \widetilde{u}_\varepsilon)^2, \tag{3.16}$$

where, for the sake of simplicity, the supra and sub indexes have been suppressed. After truncating the above expansion, we can define the following quantity

$$\Phi(\Omega_\varepsilon) = 2\alpha(\varepsilon)\int_{\Gamma_m} (u_0 - U)G, \tag{3.17}$$

where $\alpha(\varepsilon)$ comes out from the solution to the algebraic equation (3.10), namely

$$\alpha(\varepsilon) = \frac{2\pi u_0(\hat{x})}{\ln\varepsilon + 2\pi g(\hat{x})}, \tag{3.18}$$

with $\hat{x}$ used to denote the center of the ball $B_\varepsilon = B(\hat{x},\varepsilon)$. In order to avoid the calculation of g for every point $\hat{x}$ of Ω, the following simplification is frequently adopted

$$\alpha(\varepsilon) \simeq \frac{2\pi u_0(\hat{x})}{\ln\varepsilon}. \tag{3.19}$$

See, for instance, Guillaume and Idris (2002). Therefore

$$\Phi(\Omega_\varepsilon) \simeq \frac{4\pi u_0(\hat{x})}{\ln\varepsilon}\int_{\Gamma_m} (u_0 - U)G. \tag{3.20}$$

Since (3.20) depends on the point $\hat{x}$ through the function G, let us introduce an adjoint state v_0 solution to the following auxiliary variational problem

$$\left\{\begin{array}{l} \text{Find } v_0 \in \mathcal{V}, \text{ such that} \\ \displaystyle\int_\Omega \nabla v_0 \cdot \nabla\eta = -2\int_{\Gamma_m} (u_0 - U)\eta, \quad \forall \eta \in \mathcal{V}. \end{array}\right. \tag{3.21}$$

The space $\mathcal{V}$ is defined as

$$\mathcal{V} = \{\varphi \in H^1(\Omega); \varphi_{|\Gamma_0} = 0\}. \tag{3.22}$$

By setting $\eta = G$ in (3.21), we obtain

$$\int_\Omega \nabla v_0 \cdot \nabla G = -2\int_{\Gamma_m} (u_0 - U)G. \tag{3.23}$$

From the Green's identity it follows that

$$\int_{\partial\Omega} (\partial_n G)v_0 - \int_\Omega (\Delta G)v_0 = -2\int_{\Gamma_m} (u_0 - U)G. \tag{3.24}$$

Since $-\Delta G(x) = \delta(x - \hat{x})$, $\partial_n G = 0$ on Γ_m and $v_0 = 0$ on Γ_0 we conclude that

$$-2\int_{\Gamma_m} (u_0 - U)G = \int_\Omega \delta(x - \hat{x})v_0 = v_0(\hat{x}). \tag{3.25}$$

In view of (3.20) and (3.25) we get

$$\Phi(\Omega_\varepsilon) \simeq -\frac{2\pi}{\ln\varepsilon} u_0(\hat{x})v_0(\hat{x}). \tag{3.26}$$

The quantity

$$D_T\psi(\hat{x}) = u_0(\hat{x})v_0(\hat{x}), \tag{3.27}$$

is the so-called topological derivative of the shape functional $\psi(\Omega)$ at the point $\hat{x} \in \Omega$ and the function $f(\varepsilon) = -2\pi(\ln\varepsilon)^{-1}$ represents the asymptotic rate of $\psi(\Omega_\varepsilon)$ with respect to the small parameter ε. Unfortunately, the (first order) topological derivative given by (3.27) leads to unsatisfactory results for the solution to the optimization problem (2.2). Indeed, let us consider the target domain shown in Fig. 2(a), where we are going to reconstruct the small hole ω^* that appears on the top-right of the figure. After evaluating the topological derivative according to the

formula (3.27) over the domain Ω without the small hole, we obtain the result shown in Fig. 2(b). Note that the (first order) topological derivative doesn't give any information concerning the location and size of the target ω^*. This fact has also been observed by Hintermuller and Laurain (2008) in the context of electrical impedance tomography problem. See also (Novotny and Sokołowski, 2013, Ch. 4.1.5, pp. 106–109), where some examples with analytical solutions are presented.

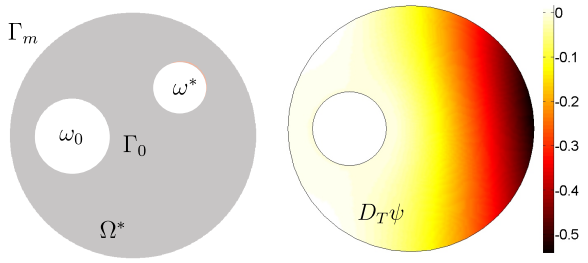

(a) target domain (b) topological derivative

FIGURE 2. Target domain Ω^* and topological derivative $D_T\psi$ evaluated over Ω.

However, we will show later that the higher order topological derivative together with the solution of (3.6) are important correction factors of the topological asymptotic expansion, leading to the solution of the inverse problem we are dealing with.

3.3. **Reconstruction Algorithm.** Let us truncate the expansion (3.13) by disregarding the remainder terms. After rearranging the obtained result, we define the following quantity

$$\Psi(\Omega_\varepsilon) = \sum_{k=1}^{M}\sum_{j=1}^{N}\int_{\Gamma_m}(u_0^k - U^k)\alpha_j^k(\varepsilon_j)G_j + \frac{1}{2}\sum_{k=1}^{M}\int_{\Gamma_m}\left(\sum_{j=1}^{N}\alpha_j^k(\varepsilon_j)G_j\right)^2. \quad (3.28)$$

Let us introduce the matrix $H \in \mathbb{R}^{N\times N}$ and the vector $d \in \mathbb{R}^N$, whose entries are respectively defined as:

$$H_{ij} := \frac{1}{2}\int_{\Gamma_m} G_iG_j \quad \text{and} \quad d_i^k := -\int_{\Gamma_m}(u_0^k - U^k)G_i. \quad (3.29)$$

From these elements, we can introduce the following function

$$\Lambda(\alpha) = -\sum_{k=1}^{M}\left[\alpha^k\cdot d^k - \frac{1}{2}H\alpha^k\cdot\alpha^k\right], \quad (3.30)$$

where $\alpha^k = (\alpha_1^k, \alpha_2^k, \ldots, \alpha_N^k)$, $\alpha = (\alpha^1, \alpha^2, \ldots, \alpha^M)$ and $\Lambda(\alpha) \equiv \Psi(\Omega_\varepsilon)$. Since G_i and G_j are linearly independent for $i \neq j$, the matrix H is positive definite. Therefore, the function (3.30) is strictly convex with respect to the variable α^k, so that there exists a unique global minimum of $\Lambda(\alpha)$ denoted by $\alpha_\star$. In fact, let us minimize $\Lambda(\alpha)$ with respect to α^k, leading to the following optimality condition:

$$\langle D_\alpha\Lambda(\alpha), \beta\rangle = -d^k\cdot\beta + H\alpha^k\cdot\beta = 0 \quad \forall\beta, \forall k. \quad (3.31)$$

Whence we conclude that

$$H\alpha^k = d^k. \quad (3.32)$$

If α^k is solution of the (3.32) then it becomes a function of $\xi = (x_1, x_2, \ldots, x_N)$, that is, $\alpha^k = \alpha^k(\xi)$. Let us comeback to (3.30) in order to obtain

$$\Lambda(\alpha(\xi)) = -\frac{1}{2}\sum_{k=1}^{M}\alpha^k(\xi)\cdot d^k. \quad (3.33)$$

The optimal locations, denoted by $x_\star$, are obtained by seeking the points that provide the lowest values for $\Lambda(\alpha(\xi))$, namely

$$x_\star = \arg\min_{\xi\in X}\Lambda(\alpha(\xi)), \quad (3.34)$$

where X is the set of admissible locations. Finally, the optimal α is simply given by $\alpha_\star = \alpha(x_\star)$.

In order to summarize the calculations presented in this section we introduce now the resulting reconstruction algorithm. Let us consider only one boundary measurement, $M = 1$ ($k = 1$). The extension for several measurements is not trivial and will be discussed later. The input of the algorithm are listed below:

- The quantity N of obstacles to be reconstructed;
- The vector $d^1 \in \mathbb{R}^N$ and the matrix $H \in \mathbb{R}^{N\times N}$, whose entries are given by (3.29).
- The number of points n_p on which the systems (3.32) are solved.

The associated output of the reconstruction algorithm is the pair $(x_\star, \alpha_\star)$, where $x_\star$ represents the optimal locations and $\alpha_\star$ can be used to obtain the optimal sizes $\varepsilon_\star$ of the hidden holes by solving the algebraic equation (3.10). In particular, let us define from (3.10) the quantity

$$\varepsilon_i(\alpha^1, \xi, N) = \exp\left\{-\frac{2\pi}{\alpha_i^1}\left[\alpha_i^1 g_i(x_i) - u_0(x_i) + \sum_{\substack{j=1\\ j\neq i}}^{N}\alpha_j^1\left(\frac{1}{2\pi}\ln\|x_i - x_j\| + g_j(x_i)\right)\right]\right\}. \quad (3.35)$$

The reconstruction process written in a pseudo-code format is shown in Algorithm 1.

Algorithm 1: Reconstruction Algorithm for $M = 1$ ($k = 1$).

Data: n_p, N, $d_i^1(x_i)$, $H_{ij}(x_i)$
Result: $\Lambda_\star$, $\alpha_\star$, $x_\star$, $\varepsilon_\star$

$\Lambda_\star \leftarrow \infty$; $\alpha_\star \leftarrow 0$; $x_\star \leftarrow 0$;
for $i_1 \leftarrow 1$, n_p **do**
  for $i_2 \leftarrow i_1 + 1$, n_p **do**
    $\vdots$
    for $i_{n_p} \leftarrow i_{n_p-1} + 1$, n_p **do**
      $d^1 \leftarrow \left(d_1^1(x_1), d_2^1(x_2), \ldots, d_N^1(x_N)\right)^\top$;
      $H \leftarrow \begin{bmatrix} H_{11}(x_1) & \cdots & H_{1N}(x_N) \\ H_{21}(x_1) & \cdots & H_{2N}(x_N) \\ \vdots & \ddots & \vdots \\ H_{N1}(x_1) & \cdots & H_{NN}(x_N) \end{bmatrix}$;
      $\alpha^1 \leftarrow H^{-1} d^1$; $\Lambda \leftarrow -\frac{1}{2} d^1 \cdot \alpha^1$;
      if $\Lambda < \Lambda_\star$ **then**
        $\Lambda_\star \leftarrow \Lambda$;
        $\alpha_\star \leftarrow \alpha^1$;
        $x_\star \leftarrow \xi$;
      end if
    end for
  end for
end for
$\varepsilon_\star \leftarrow \varepsilon_i(\alpha_\star, x_\star, N)$;
return $\Lambda_\star$, $\alpha_\star$, $x_\star$, $\varepsilon_\star$.

The complexity order of Algorithm 1 has been analysed by Machado et al. (2016), where a multigrid strategy has been proposed, which allows for dealing with a high number N of hidden anomalies.

4. Numerical Results

In this section some numerical results are presented in order to demonstrate the effectiveness of the proposed reconstruction Algorithm 1. In the numerical examples the domain Ω is given by a circle centered at $(0, 0)$ and with unit radius. In addition, Ω has a hole ω_0 centered at $(-0.5, 0)$ and with radius 0.3. See Fig. 3.

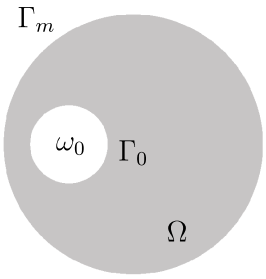

Figure 3. Domain Ω.

The target domain Ω^* is given by $\Omega \setminus \overline{\omega^*}$, where $\omega^* = \bigcup_{l=1}^N \omega_l^*$ represents the hidden set of obstacles within the domain Ω^*. We want to reconstruct the set ω^* from partial boundary measurement on the boundary Γ_m. Therefore, the idea is to exciting the body Ω^* with a set of given fluxes Q^k, $k = 1, .., M$, and measure the associated potentials U^k on Γ_m. Then, the same set of fluxes Q^k is applied to the body Ω, allowing for computing u_0^k solution of problem (2.3). From U^k and u_0^k, the minimization problem (2.2) is solved with help of the reconstruction Algorithm 1. The synthetic set of boundary measurements U^k is obtained from the trace on Γ_m of the solution to the following boundary value problem depending on the set of boundary data Q^k

$$\begin{cases} \Delta u^k &= 0 \quad \text{in} \quad \Omega^* = \Omega \setminus \overline{\omega^*}, \\ u^k &= 0 \quad \text{on} \quad \Gamma_0, \\ u^k &= 0 \quad \text{on} \quad \partial\omega^*, \\ -\partial_n u^k &= Q^k \quad \text{on} \quad \Gamma_m. \end{cases} \tag{4.1}$$

The above problem (4.1) and the auxiliaries boundary value problems (2.3) and (3.6) are solved using the Finite Element Method. The domains Ω^* and Ω are discretized with three-node finite elements. The mesh is generated from the Delaunay triangulation algorithm. The functions u_0^k, U^k and g_j are computed over this mesh. From these functions the systems (3.32) can be numerically solved at any point of the mesh. Finally, the combinatorial search (3.34) is performed, leading to the optimal solution $(x_\star, \varepsilon_\star)$. Therefore, we define a *sub-mesh* of the original *mesh* where (3.32) and (3.34) are evaluated. This sub-mesh is chosen in order to have a good compromise between resolution and computational cost (Canelas et al., 2014). In the following numerical experiments the target ω^* is represented by red lines, while the reconstruction result is represented by blue lines. In all examples we consider only one boundary measurement ($k = 1$) denoted by U obtained from a constant boundary excitation $Q = 1$, except in the last example where additional boundary measurements are considered.

4.1. **Example 1.** In this first example, we consider the sensitivity of the reconstruction algorithm with respect to the sub-mesh. Let us consider the domain Ω^* shown in Fig. 4, which presents a circular obstacle ω^* located at the point $x^* = (0.4, 0.4)$ and with radius $\varepsilon^* = 0.1$. We start with a sub-mesh of 197 points uniformly distributed within Ω. Then this sub-mesh is uniformly refined twice, leading respectively to 734 and 2828 points. The results associated with each discretization are respectively shown in Figs. 5(a), 5(b) and 5(c). Finally, the last result shown in Fig. 5(d) is also obtained with 734 points, but with one of them coinciding with the center $x^* = (0.4, 0.4)$.

From an inspection of the results presented in Fig. 5, we observe that the more the sub-mesh is refined the better is the reconstruction. Of course, the best result is obtained when x^* belongs to the sub-mesh. For a quantitative analysis of the results obtained, see Table 1. See also the convergence curves for $\|x^* - x_\star\|$ and $|\varepsilon^* - \varepsilon_\star|$ in Fig. 6.

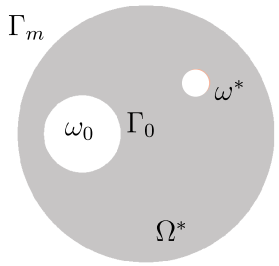

FIGURE 4. Example 1: Target Ω^*.

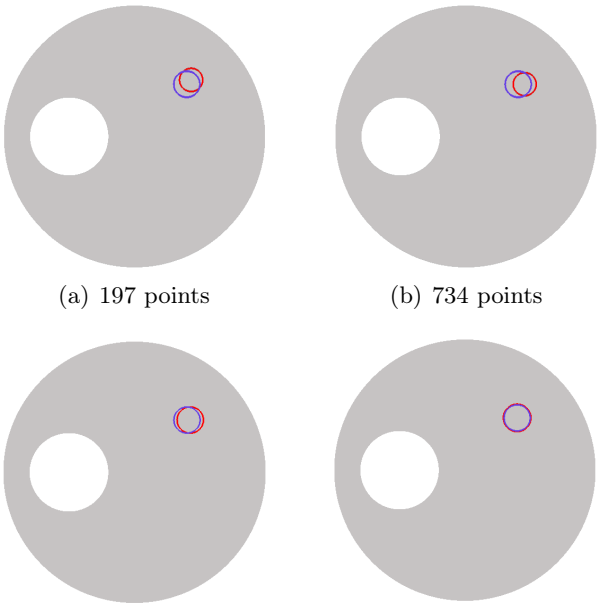

(a) 197 points (b) 734 points

(c) 2828 points (d) 734 points*

FIGURE 5. Example 1: Results obtained for different sub-meshes. *In (d) the center of the obstacle coincides with one of the sub-mesh points.

TABLE 1. Example 1: Results obtained for different sub-meshes.

Points	$x_\star$	$\varepsilon_\star$
197	(0.433, 0.433)	0.089
734	(0.450, 0.400)	0.088
2828	(0.425, 0.400)	0.101
*734	(0.400, 0.400)	0.106

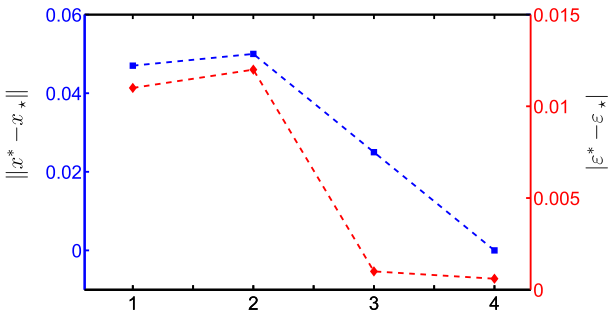

FIGURE 6. Example 1: Convergence curves.

In all further examples the sub-mesh is generated first. Then it is uniformly refined twice by dividing each original element into four new elements in each step of the mesh refinement. Finally, the resulting finer mesh is used to discretize Ω^* and Ω. In order to show different features of the reconstruction Algorithm 1, from now on we assume that the center of each obstacle to be reconstructed coincides with one point of the sub-mesh.

4.2. **Example 2.** Now the synthetic boundary measurement U is corrupted with White Gaussian Noise (WGN), denoted by μ. The idea is to verify the robustness of the reconstruction Algorithm 1 with respect to noisy data. The target domain Ω^* has three hidden circular obstacles, ω_1^*, ω_2^* and ω_3^*, as shown in Fig. 7. The center as well as the radius of each obstacle is shown in Table 2. The level of noise is set as $\mu \in \{0\%, 1\%, 5\%, 10\%\}$. The result obtained associated with each level of noise is presented in Fig. 8. For a quantitative comparison of the results for $\mu = 0\%, 1\%, 5\%$ and 10% see Tables 3 and 4. As expected, the higher is the level of noise the worst is the reconstruction. In any case, the reconstruction can be considered satisfactory even for a high level of noise.

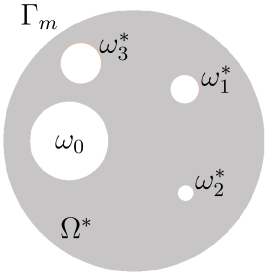

FIGURE 7. Example 2: Target Ω^*.

TABLE 2. Example 2: Location and sizes of the obstacles.

	ω_1^*	ω_2^*	ω_3^*
x^*	$(0.400, 0.400)$	$(0.400, -0.400)$	$(-0.400, 0.600)$
ε^*	0.100	0.050	0.150

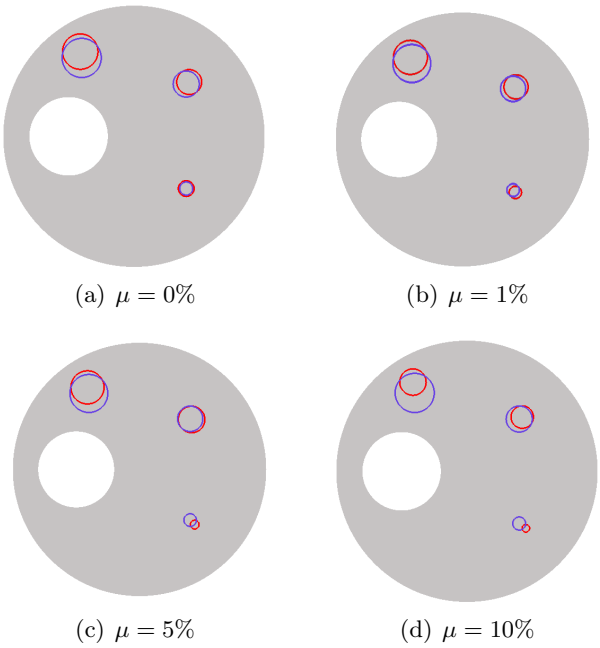

(a) $\mu = 0\%$ (b) $\mu = 1\%$

(c) $\mu = 5\%$ (d) $\mu = 10\%$

FIGURE 8. Example 2: Results obtained for different values of noise μ.

TABLE 3. Example 2. Result for WGN $\mu = 0\%$ and 1%

		Different values of noise μ	
		0%	1%
ω_1^*	$x_\star$	$(0.423, 0.415)$	$(0.423, 0.415)$
	$\varepsilon_\star$	0.096	0.095
ω_2^*	$x_\star$	$(0.400, -0.400)$	$(0.418, -0.418)$
	$\varepsilon_\star$	0.061	0.049
ω_3^*	$x_\star$	$(-0.411, 0.648)$	$(-0.411, 0.648)$
	$\varepsilon_\star$	0.136	0.135

TABLE 4. Example 2. Result for WGN $\mu = 5\%$ and 10%

		Different values of noise μ	
		5%	10%
ω_1^*	$x_\star$	$(0.411, 0.394)$	$(0.423, 0.415)$
	$\varepsilon_\star$	0.105	0.086
ω_2^*	$x_\star$	$(0.435, -0.435)$	$(0.451, -0.436)$
	$\varepsilon_\star$	0.035	0.029
ω_3^*	$x_\star$	$(-0.411, 0.648)$	$(-0.414, 0.683)$
	$\varepsilon_\star$	0.135	0.131

4.3. **Example 3.** In this numerical experiment we want to seek for the number N^* of unknown obstacles. The target domain Ω^* is shown in Fig. 9(a), which has two obstacles ω_1^* and ω_2^* respectively located at the points $x_1^* = (0.6, -0.6)$ and $x_2^* = (-0.2, 0.8)$ with radii $\varepsilon_1^* = \varepsilon_2^* = 0.1$. We start the reconstruction Algorithm 1 by setting $N = 1$. Then, the number N is increased until finding a trial ball of negligible size, allowing for infer that the optimal number of obstacles is given by $N_\star = N - 1$. The results are shown in Figs. 9(b), 9(c) and 9(d). For $N = 1$ the solution is clearly far from the target (Fig. 9(b)). For $N = 2$ the locations and radii are satisfactorily reconstructed (Fig. 9(c)). Finally, for $N = 3$ there is an additional trial ball with negligible size, namely 5×10^{-6} (Fig. 9(d)). Therefore, we can infer that the optimal solution is the one shown in Fig. 9(c), where $N_\star = 2$. Note that such a procedure is non-iterative, since the solutions for different number of trial balls N are completely independent of each other. In addition, we can start the Algorithm 1 based on the assumption that there exists $N > N^*$ and find a number $(N - N^\star)$ of trial balls with negligible sizes in just one shot.

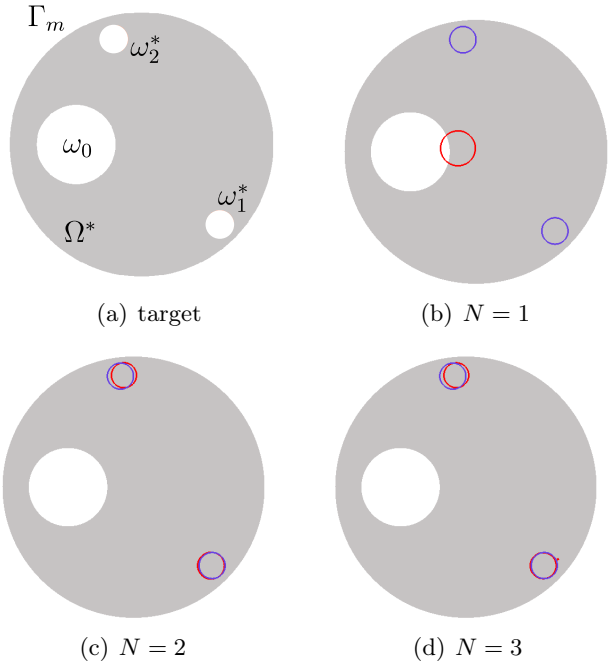

(a) target (b) $N = 1$

(c) $N = 2$ (d) $N = 3$

FIGURE 9. Example 3: Target Ω^* and results obtained for different number of trial balls.

4.4. **Example 4.** Let us consider the reconstruction of arbitrary shaped obstacles. In particular, the target domain Ω^* shown in Fig. 10(a) has two obstacles, where ω_1^* is a square and ω_2^* is a triangle. Their respective barycenters are located at

$x_1^* = (0.400, -0.400)$ and $x_2^* = (0.490, 0.270)$, while the associated areas are given by $A_1^* = 0.04$ and $A_2^* = 0.03$. The idea is to approximate the obstacles by a number of trial balls. The result obtained is shown in Fig. 10(b). The quantitative results can be seen in Table 5, where both the barycenters and areas are well reconstructed.

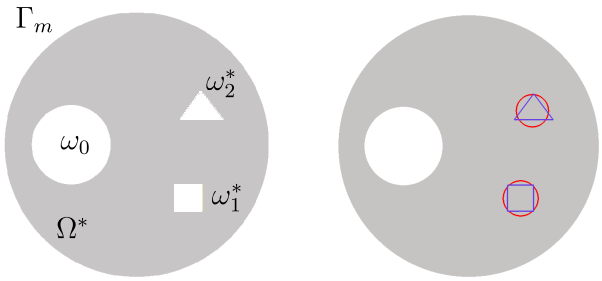

(a) target (b) result

FIGURE 10. Example 4: Target Ω^* and result obtained.

TABLE 5. Example 4: Location $x_\star$ and areas $A_\star$ of the obstacles.

	ω_1^*	ω_2^*
$x_\star$	$(0.400, -0.400)$	$(0.490, 0.270)$
$A_\star$	0.057	0.048

4.5. **Example 5.** In this last numerical experiment the target domain Ω^* has three hidden circular obstacles, ω_1^*, ω_2^* and ω_3^*, as shown in Fig. 11, with radii $\varepsilon_1^* = \varepsilon_2^* = \varepsilon_3^* = 0.1$ and centers at $x_1^* = (0.2, 0.4)$, $x_2^* = (0.2, -0.4)$ and $x_3^* = (0.75, 0)$. The result obtained is shown in Fig. 12(a). We note that in this case the reconstruction Algorithm 1 fails.

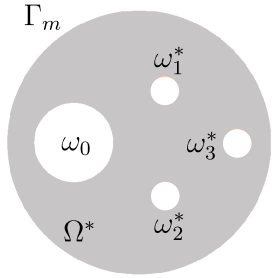

FIGURE 11. Example 5: Target Ω^*.

In order to improve the result, let us add more boundary measurements. In particular, we consider a set of five boundary excitations on Γ_m given by $Q^1 = 1$, $Q^2 = x$, $Q^3 = y$, $Q^4 = (x+y)/\sqrt{2}$ and $Q^5 = (x-y)/\sqrt{2}$. Then, the target Ω^* is reconstructed again with help of five associated boundary measurements on Γ_m, namely U^1, U^2, U^3, U^4 and U^5. In the case of more than one boundary measurement the reconstruction Algorithm 1 returns the optimal locations $x_\star$ and optimal $\alpha_\star$. From $x_\star$ and $\alpha_\star$ we can obtain the optimal radii $\varepsilon_\star$ by solving equation (3.10). This is actually trivial for $M = 1$, leading to (3.35). However, for $M > 1$ the constraint (3.10) leads to a system of non-linear algebraic equations, which cannot be solved explicitly. Therefore, in order to avoid such a difficulty, we start by finding the optimal centers $x_\star$ using all available information, namely $M = 5$. Then, for fixed $x_\star$, we compute the optimal radii $\varepsilon_\star$ from (3.35) by taking into account just one boundary measurement $M = 1$, namely U^1. The result obtained from this procedure is shown in Fig. 12(b), where the reconstruction is quite good.

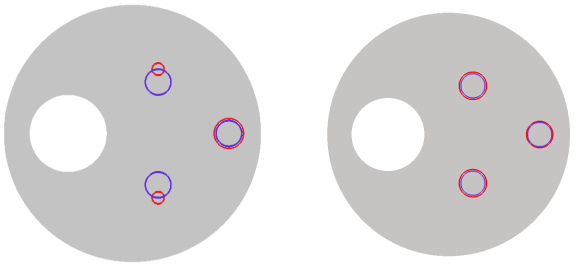

(a) $M = 1$ (b) $M = 5$

FIGURE 12. Example 5: Results obtained for different number of partial boundary measurements.

5. Conclusions

In this paper a new method for solving an inverse obstacle reconstruction problem from partial boundary measurements has been proposed. In particular, for a given boundary excitation, we have determined the quantity, locations and sizes of a number of holes embedded within a geometrical domain, from partial boundary measurements related to such an excitation. Since the associated inverse problem is written in the form of an ill-posed and over-determined boundary value problem, we have rewritten it as an optimization problem where a shape functional measuring the misfit between the boundary measurement and the solution to an auxiliary boundary value problem has been minimized with respect to a set of ball-shaped holes. The second order topological derivative concept was used for solving the resulting topology optimization problem, leading to a non-iterative second order reconstruction algorithm, which is very robust with respect to noisy data and also free of initial guess. In particular, we have recovered a term g_j frequently disregarded in the literature, which has

been shown to be crucial for solving the inverse problem we are dealing with. In addition, some numerical results were presented, showing the effectiveness of proposed reconstruction algorithm. However, the approximation of the solution by a finite number of ball-shaped holes can be seen as a limitation of our approach. On the other hand, the reconstruction obtained may serve as an initial guess for other well-established iterative methods (Leitão and Baumeister, 2005). Finally, the model problem here considered to introduce the ideas can be easily extended to more realistic situations, like the one concerning obstacles reconstruction in fluid flow problems from partial boundary measurements (Alvarez et al., 2005).

Acknowledgements

This research was partly supported by CNPq (Brazilian Research Council), CAPES (Brazilian Higher Education Staff Training Agency) and FAPERJ (Research Foundation of the State of Rio de Janeiro). These supports are gratefully acknowledged.

References

C. Alvarez, C. Conca, L. Friz, O. Kavian, and J. H. Ortega. Identification of immersed obstacles via boundary measurements. *Institute of Physics Publishing Inverse Problems*, 21(5):1531–1552, 2005.

C. J. S. Alves and T. Ha-Duong. Inverse scattering for elastic plane cracks. *Inverse Problems*, 15(1):91–97, 1999.

H. Ammari and H. Kang. *Reconstruction of small inhomogeneities from boundary measurements*. Lectures Notes in Mathematics vol. 1846. Springer-Verlag, Berlin, 2004.

S. Amstutz and N. Dominguez. Topological sensitivity analysis in the context of ultrasonic nondestructive testing. *Engineering Analysis with Boundary Elements*, 32(11):936–947, 2008.

S. Amstutz, I. Horchani, and M. Masmoudi. Crack detection by the topological gradient method. *Control and Cybernetics*, 34(1):81–101, 2005.

S. Andrieux, A. B. Abda, and H. D. Bui. Reciprocity principle and crack identification. *Inverse Problems*, 15:59–65, 1999.

M. Bonnet. Topological sensitivity for 3d elastodynamic and acoustic inverse scattering in the time domain. *Computer Methods in Applied Mechanics and Engineering*, 195(37-40):5239–5254, 2006.

M. Bonnet. Higher-order topological sensitivity for 2-D potential problems. *International Journal of Solids and Structures*, 46(11–12):2275–2292, 2009.

M. Burger. A level set method for inverse problems. *Inverse Problems*, 17:1327–1356, 2001.

A. Canelas, A. Laurain, and A. A. Novotny. A new reconstruction method for the inverse potential problem. *Journal of Computational Physics*, 268:417–431, 2014.

A. Canelas, A. Laurain, and A. A. Novotny. A new reconstruction method for the inverse source problem from partial boundary measurements. *Inverse Problems*, 31(7):075009, 2015.

Y. Capdeboscq and M. S. Vogelius. A general representation formula for boundary voltage perturbations caused by internal conductivity inhomogeneities of low volume fraction. *Mathematical Modelling and Numerical Analysis*, 37(1):159–173, 2003a.

Y. Capdeboscq and M. S. Vogelius. Optimal asymptotic estimates for the volume of internal inhomogeneities in terms of multiple boundary measurements. *Mathematical Modelling and Numerical Analysis*, 37(2):227–240, 2003b.

A. Carpio and M-L. Rapún. Solving inhomogeneous inverse problems by topological derivative methods. *Inverse Problems*, 24(4):045014, 2008.

F. Caubet and M. Dambrine. Localization of small obstacles in stokes flow. *Inverse Problems*, 28(10):1–31, 2012.

D. J. Cedio-Fengya, S. Moskow, and M. S. Vogelius. Identification of conductivity imperfections of small diameter by boundary measurements. Continuous dependence and computational reconstruction. *Inverse Problems*, 14(3):553–595, 1998.

D. Colton and A. Kirsch. A simple method for solving inverse scattering problems in the resonance region. *Inverse Problems*, 12:383–393, 1996.

D. Colton, H. Haddar, and M. Piana. The linear sampling method in inverse electromagnetic scattering theory. *Inverse Problems*, 19:S105–S137, 2003.

J. Rocha de Faria and A. A. Novotny. On the second order topologial asymptotic expansion. *Structural and Multidisciplinary Optimization*, 39(6):547–555, 2009.

K. Doel, U. Ascher, and A. Leitao. Multiple level sets for piecewise constant surface reconstruction in highly ill-posed problems. *Journal of Scientific Computing*, 43:44–66, 2010.

N. Dominguez, V. Gibiat, and Y. Esquerre. Time domain topological gradient and time reversal analogy: an inverse method for ultrasonic target detection. *Wave Motion*, 42:31–52, 2005.

O. Dorn and D. Lesselier. Level set methods for inverse scattering. *Inverse Problems*, 22:R67–R131, 2006.

G. R. Feijóo, A. A. Oberai, and P. M. Pinsky. An application of shape optimization in the solution of inverse acoustic scattering problems. *Inverse*

Problems, 20:199–228, 2004.

P. Guillaume and K. Sid Idris. The topological asymptotic expansion for the Dirichlet problem. *SIAM Journal on Control and Optimization*, 41(4):1042–1072, 2002.

B. B. Guzina and M. Bonnet. Small-inclusion asymptotic of misfit functionals for inverse problems in acoustics. *Inverse Problems*, 22(5):1761–1785, 2006.

B. B. Guzina and M. Bonnet. Topological derivative for the inverse scattering of elastic waves. *Quarterly Journal of Mechanics and Applied Mathematics*, 57(2): 161–179, 2004.

B. B. Guzina and I. Chikichev. From imaging to material identification: a generalized concept of topological sensitivity. *Journal of the Mechanics and Physics of Solids*, 55(2):245–279, 2007.

M. Hintermüller and A. Laurain. Electrical impedance tomography: from topology to shape. *Control and Cybernetics*, 37(2): 913–933, 2008.

M. Hintermüller, A. Laurain, and A. A. Novotny. Second-order topological expansion for electrical impedance tomography. *Advances in Computational Mathematics*, 36(2):235–265, 2012.

V. Isakov. *Inverse source problems.* American Mathematical Society, Providence, Rhode Island, 1990.

R. Kohn and M. Vogelius Identification of an unknow conductivity by means of measurements at the boundary. *Inverse Problems*, 14:113–123, 1984.

V. A. Kozlov, V. G. Maz'ya, and A. B. Movchan. *Asymptotic analysis of fields in multi-structures.* Clarendon Press, Oxford, 1999.

R. Kress. Integral equation methods in inverse obstacle scattering. *Engineering Analysis with Boundary Elements*, 15:171–179, 1995.

R. Kress. Inverse elastic scattering from a crack. *Inverse Problems*, 12:667–684, 1996.

A. Leitão and J. Baumeister. *Topics in Inverse Problems.* IMPA Mathematical Publications, Rio de Janeiro, 2005.

V. Liepa, F. Santosa, and M. Vogelius. Crack determination from boundary measurements - reconstruction using experimental data. *Joumal of Nondestrunctive Evaluation*, 12(3), 1993.

A. Litman. Reconstruction by level sets of n-ary scattering obstacles. *Inverse Problems*, 21:S131–S152, 2005.

T. J. Machado, J. S. Angelo and A. A. Novotny. *A new one-shot pointwise source reconstruction method.* Mathematical Methods in the Applied Sciences,1099-1476, 2016.

V. G. Maz'ya, S. A. Nazarov and B. A. Plamenevskij. *Asymptotic theory of elliptic boundary value problems in singularly perturbed domains. Vol. I ,Operator Theory: Advances and Applications.* Translated from the German by Georg Heinig and Christian Posthoff, Birkhäuser Verlag, Volume 111, 2000.

N. Nishimura and S. Kobayashi. Determination of cracks having arbitrary shapes with the boundary integral equation method. *Engineering Analysis with Boundary Elements*, 15:189–195, 1994.

A. A. Novotny and J. Sokołowski. *Topological derivatives in shape optimization.* Interaction of Mechanics and Mathematics. Springer-Verlag, Berlin, Heidelberg, 2013.

A. I. Prilepko. Über existenz und eindeutigkeit von lösungen inverser probleme der potentialtheorie. *Mathematische Nachrichten*, 63:135–153, 1974.

J. Sokołowski and A. Żochowski. On the topological derivative in shape optimization. *SIAM Journal on Control and Optimization*, 37(4):1251–1272, 1999.

(S. S. Rocha & A.A. Novotny) Laboratório Nacional de Computação Científica LNCC/MCT, Coordenação de Matemática Aplicada e Computacional, Av. Getúlio Vargas 333, 25651-075 Petrópolis - RJ, Brasil

E-mail address: novotny@lncc.br